

Photoconductivity of Self-Assembled Porphyrin Nanorods

Alexander D. Schwab,^{†,‡} Deirdre E. Smith,^{†,§} Brooks Bond-Watts,[†]
Danvers E. Johnston,[§] James Hone,^{||} Alan T. Johnson,[§] Julio C. de Paula,^{*,†} and
Walter F. Smith^{*,‡}

Departments of Chemistry and Physics, Haverford College,
Haverford, Pennsylvania 19041, Department of Physics and Astronomy,
University of Pennsylvania, Philadelphia, Pennsylvania 19104, and Department of
Mechanical Engineering, Columbia University, New York, New York 10027

Received April 19, 2004; Revised Manuscript Received May 17, 2004

ABSTRACT

The photoconductivity of nanorods self-assembled from meso-tetrakis(4-sulfonatophenyl)porphine is described. The nanorods are insulating in the dark. Upon illumination with 488 nm light, the nanorods become photoconductive, exhibiting a rapid turn on/off (<100 ms) of the current when the light is turned on/off. This photoconductivity grows over hundreds of seconds with light exposure and decays slowly when the light is off. The nanorods can be trained via an applied bias to exhibit a short-circuit photocurrent (with corresponding open-circuit photovoltage) that flows in the direction opposite that of the training bias. A qualitative model is proposed, in which conduction occurs through the tightly coupled LUMOs of close-packed porphyrin molecules.

Introduction. Of the options available to manufacture nanometer-sized objects, none is more versatile than molecular self-assembly, which is driven by noncovalent intermolecular interactions. Porphyrins offer several attractive features for molecular self-assembly^{1–18} including a large, flat, conjugated central tetrapyrrole macrocycle that can be decorated with hydrophobic and hydrophilic substituents. The assembly of porphyrin aggregates can be promoted by intermolecular π - π interactions, which are known to be a significant driving force for self-assembly of a number of materials.^{2,8,13,15,19} Second, with appropriate choice of substituents, noncovalent self-assembly can occur via intermolecular electrostatic interactions,¹² hydrogen bonding,^{9,11,15,18} and metal coordination.^{3,4,8,10,11,14–18} Additionally, substituents can impart desired properties on the molecule and/or the assembly. As a result, a wide variety of nanometer-sized self-assembled structures have been described using porphyrins, including nanoporous solid materials,^{1–4} rigid and ordered monolayers,^{5,6} rings,⁷ columnar stacks,⁸ linear tapes,^{9–11} rigid rods,¹² nanoparticles,¹³ cyclic tetramers,^{14,15} pentamers,¹⁶ cyclic hexamers,¹⁷ and nonamers.^{8,18}

Porphyrins absorb certain wavelengths of visible light strongly, and the close molecular packing in self-assembled porphyrin arrays offers the possibility for intermolecular

transfer or delocalization of the excitation energy. Light absorption and energy transfer by closely packed chromophores are central to the mechanism of light harvesting in photosynthetic organisms.²⁰ A relevant example is the chlorosome, the light harvesting apparatus of the green photosynthetic bacterium *Chloroflexus aurantiacus*, which contains rod-shaped aggregates of bacteriochlorophyll *c* with diameters of 5.2 nm. The bacteriochlorophyll *c* molecules are chemically similar to porphyrins and are closely packed to allow for efficient energy capture and transfer.^{21,22}

Various macroscopic devices have been fabricated from porphyrins that are photoconductive,^{23,24} photovoltaic,^{25–28} or capable of light mediated charge storage.²⁹ In this report, we present results illustrating the two remarkable facets of porphyrin molecules discussed so far: their ability to self-assemble into nanometer sized structures and their ability to transport electrical charge. In a previous study, we showed that the porphyrin meso-tetrakis(4-sulfonatophenyl)porphine (TPPS₄) self-assembles in acidic aqueous solution into rods with a well-defined height of 3.8 ± 0.3 nm and lengths ranging from 0.2 to 2 μm .¹² These aggregates exhibit a characteristic electronic transition with a peak at 492 nm. In this study, these porphyrin nanorods were deposited onto an array of electrodes spaced 350 nm apart, and the electrical properties of the nanorods were measured while they were exposed to light with a wavelength of 488 nm. The nanorods display an intriguing array of photoconductive behaviors, demonstrating that nanometer-sized pho-

* Corresponding authors. E-mail: jdepaula@haverford.edu and wsmith@haverford.edu.

[†] Department of Chemistry, Haverford College.

[‡] Department of Physics, Haverford College.

[§] University of Pennsylvania.

^{||} Columbia University.

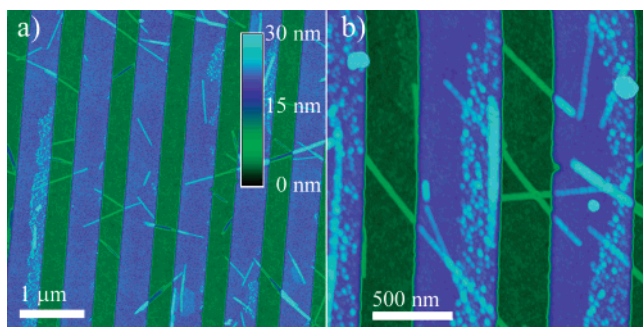


Figure 1. AFM images showing porphyrin nanorods (light green) bridging the 350 nm gap between the interdigitated electrodes (blue).

toelectronic devices can be fabricated using self-assembled porphyrinic materials.

Experimental Methods. AuPd interdigitated metal electrodes (15 nm thick on a 3 nm Cr adhesion layer) were fabricated by electron beam lithography on p-doped Si substrates with a 400 nm oxide layer. Solutions of aggregated TPPS₄ were prepared as previously described.¹² Immediately prior to immersion of the electrode substrates in aggregate solution, the substrates were cleaned for 30 min in a UV/ozone cleaner (Bioforce Nanosciences Tipcleaner) and subsequently baked in a 300 °C oven for 1 h in air. The electrode substrates were then immersed in the aggregate solution for 2–3 h, quickly transferred to a spin coating platform, and then rapidly dried by spinning the substrates for 60 s at 4000 rpm. The depositions of nanorods as well as the electrode geometries were then verified by AFM imaging of the samples. All AFM images were acquired using a Digital Instruments Bioscope operated in tapping mode at ~300 kHz.

Conductance measurements were performed using a Keithley 6517A electrometer, which contains a programmable voltage source set to +0.50 V, 0.00 V, or –0.50 V for all measurements except *I*–*V* curves. Illumination was provided by a Spectra Physics 177-G02 Ar ion laser, with a monochromator at the output to select the 488.0 nm wavelength. The laser beam was directed through a small fixed iris and was focused onto the sample with an achromatic doublet lens (focal length = 300 mm) to a final beam diameter of ~0.3 mm. To measure light power in situ, a small fraction of the beam was reflected onto a calibrated, amplified Si photodiode (ThorLabs PDA50). The beam intensity was calculated by simply dividing the beam power by the spot size. The focused spot was centered onto the interdigitated electrodes as observed with an overhead stereomicroscope. All conductivity measurements were performed under argon gas, with a measured O₂ level inside the measurement chamber of 0.4–0.6% (Vernier O₂–BTA O₂ gas sensor).

Results. AFM images obtained from the interdigitated electrodes after immersion in the porphyrin aggregate solutions are shown in Figure 1. The AFM images clearly show the presence of porphyrin nanorods and that these nanorods bridge the gap between the electrodes.

To estimate the number of nanorods bridging the two electrodes, fifteen AFM images, similar to that shown in

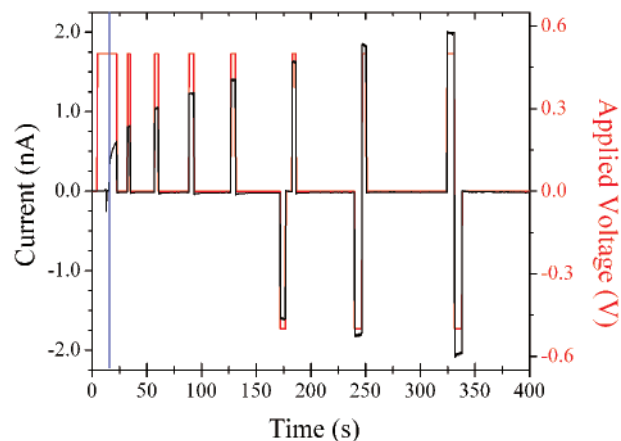


Figure 2. Measured current (in black) as a function of applied voltage, V_{app} (in red), demonstrating a slow increase in photoconductivity of porphyrin nanorods (see Figure 1) under continuous light exposure. The blue line indicates the time the sample was exposed to 488 nm, 11.0 kW m⁻² light.

Figure 1a, were acquired from different areas of the electrodes. The nanorods bridging the electrode gaps in these fifteen images were counted, and the resulting number of nanorods was normalized to the total electrode length appearing in all fifteen images. From this procedure, it was determined that the average spacing between nanorods is 1.1 μm. The electrode arrays used in this study contain 98 gaps, each 56 μm long. Therefore, we estimate that approximately 6100 nanorods span our electrodes.

In our previous work,¹² the porphyrin nanorods used in this study were shown to have a well-defined height of 3.8 ± 0.3 nm. However, the widths of the nanorods are more difficult to determine. The average nanorod cross section indicates that the nanorod has a flat top with a width of ~10 nm, meaning that the nanorods have a rectangular or a trapezoidal cross section rather than a circular cross section. Similar observations were made using a variety of standard AFM tips as well as tips based on very sharp carbon asperities (“Hi-res” tips, MikroMasch Inc.). Though a crystal structure has not been determined for the porphyrin used in this study, crystallographic studies on similar porphyrin molecules yield theoretical densities between 1.2 and 1.4 g cm⁻³.^{30–32} Assuming a density for our porphyrin nanorods of 1.2 g cm⁻³, and using the nanorod dimensions quoted above, we estimate that a total of 9.4 × 10⁻¹⁴ g of porphyrin material bridges the gap between the electrodes, corresponding to 5.6 × 10⁷ porphyrin molecules contributing to the conductance studies presented in this paper. All measurements reported here were from a single sample for internal consistency, but they are representative of similar results obtained on several samples.

The porphyrin nanorods were insulating in the dark; at a bias voltage of 0.5 V, a current of less than 0.2 pA was observed through our array of 6100 nanorods. However, under illumination several distinct photoconduction phenomena were observed. In Figure 2, a series of voltage pulses were applied under continuous illumination. The measured currents coinciding with the voltage pulses showed that the

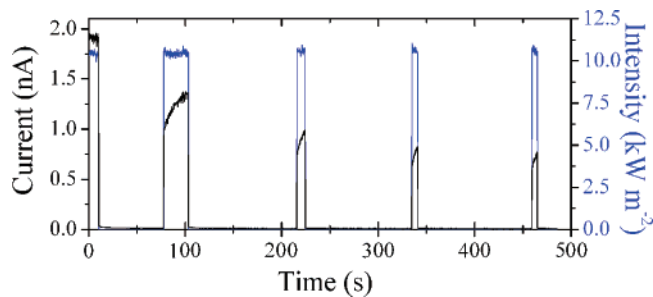


Figure 3. Photoconductivity decline probed by using short duration light pulses and a constant applied voltage ($V_{\text{app}} = 0.50$ V). The measured current (black) that coincides with the light intensity (blue) pulses indicates slowly decreasing photoconductivity in the absence of constant illumination.

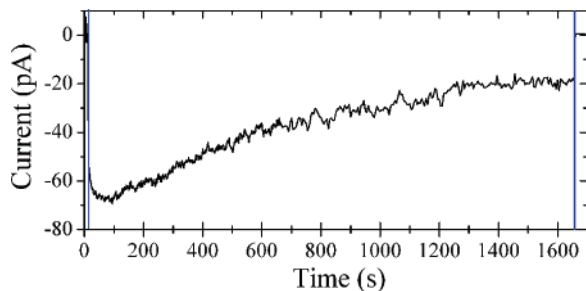


Figure 4. Short-circuit photocurrent produced by exposing the sample to 488 nm light (10.6 kW m^{-2}) with the sample's electrodes short circuited. The first and second vertical blue lines indicate the times the light source was turned on and off, respectively. Prior to this measurement, positive currents of 0.6 to 1.0 nA were passed through the sample for roughly 1000 s.

photoconductivity slowly increased upon light exposure and did not require constant applied voltage or current flow.

When light was removed, the photoconductivity (defined as conductivity under illumination) slowly declined. Measurement of this decline is challenging because light exposure is necessary to produce photoconductivity and hence to measure it. Additionally, as shown in Figure 2, light exposure increases the photoconductivity. The key, therefore, is to limit light exposure by using short duration pulses of light to probe the photoconductivity under a constant applied voltage as illustrated in Figure 3. The average current measured during the light pulse decreased from pulse to pulse, indicating that the photoconductivity slowly decreased, though it also increased during the duration of the each probing light pulse. Figure 3 also shows that the current turned on and off rapidly when the light was turned on and off; with the characteristic turn on/off time being less than the instrumental resolution of <100 ms.

When the bias voltage was reduced to zero after a set of photoconductivity measurements, a zero-bias photocurrent was observed that flowed in the opposite direction of the previously applied bias voltage. This short-circuit photocurrent only flowed when the sample was exposed to light as demonstrated in Figure 4. The magnitude of this current was about 10 times smaller than the photocurrent with 0.5 V bias applied. Prior to the data presented in Figure 4, currents of 0.6 to 1.1 nA were passed through the sample for a total of roughly 1000 s by exposing the sample to a light intensity

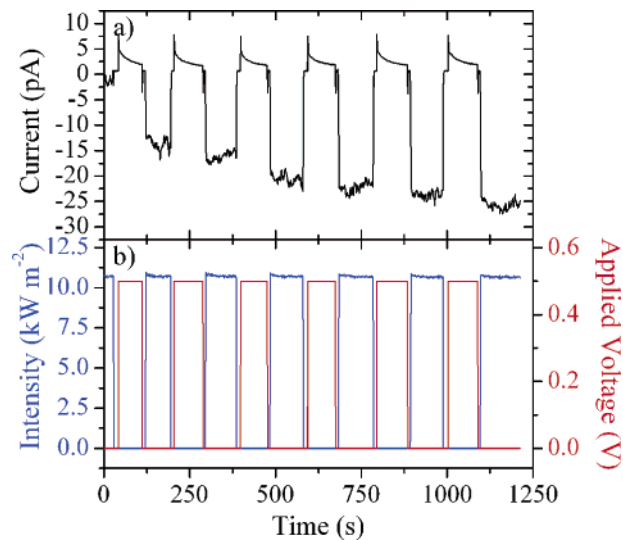


Figure 5. Illustration of the training effect of the short-circuit photocurrent. (a) The current was measured as (b) the applied voltage (in red) was switched between 0.00 or 0.50 V and as the 488.0 nm light intensity (in blue) was switched on and off. A series of alternating light and applied voltage pulses were applied to the sample, each 1 min in duration. The negative short circuit photocurrent, observed when the sample electrodes are short-circuited ($V_{\text{app}} = 0$) and illuminated (intensity > 0), increased in magnitude after each application of applied voltage, illustrating the short-circuit photocurrent training effect.

of 10.6 kW m^{-2} with $V_{\text{app}} = 0.5$ V. The light source was then blocked, and the terminals short-circuited. Data collection began and the light was unblocked after several seconds, indicated by the first vertical, blue line in Figure 4. The magnitude of the resulting short-circuit photocurrent quickly increased upon light exposure and then slowly decreased in magnitude. The light source was again blocked after ~ 1650 s to illustrate further that light is necessary for the generation of this photocurrent.

The short-circuit photocurrent can be trained to occur in either direction. Forcing a positive current through the sample via application of a positive bias voltage led to a negative short-circuit photocurrent when the bias was removed and vice-versa. Additionally, the training of the short-circuit photocurrent did not require simultaneous light and applied bias voltage, but could also be accomplished by alternating applied voltage and light exposure, as shown in Figure 5. The sample was subjected to alternating pulses of light exposure and applied voltage, each 1 min in length. The application of positive applied voltages slowly built up a negative short-circuit photocurrent. Nanorod covered electrodes that are kept in the dark, however, did not develop a short-circuit photocurrent regardless of how long a voltage was applied to the sample. This experiment demonstrates that the training of the short-circuit photocurrent requires light exposure and applied voltage, but not simultaneously.

As might be expected, we could also measure an open-circuit photovoltage that scaled with the short-circuit photocurrent. For example, an open-circuit photovoltage of -15.3 mV was observed with a corresponding short-circuit photocurrent of -60 pA.

Current–voltage characteristics obtained between -0.5 and $+0.5$ V consistently showed a linear relationship, with a resistance of $2.4 \times 10^8 \Omega$ under the 11.0 kW m^{-2} intensity used here. To obtain meaningful I – V curves, it was necessary to wait about 1 h for the photoconductivity to complete the slow growth phase and stabilize.

Discussion. First we consider whether the currents observed in our porphyrin nanorods can be supplied by electrochemical oxidation or reduction reactions, or by the release of stored charge. The ability of porphyrins to store charge for long periods of time has been illustrated in studies on $1 \mu\text{m}$ thick films of zinc-octakis(b-decoxyethyl) porphyrin. The stored charge could be released by subsequent light exposure under short-circuit conditions.^{28,29} For our experiment, assuming one electron contributed by each porphyrin molecule, a maximum charge of 9.0×10^{-12} A s, i.e., 9.0 pA for 1 s, could be supplied by such mechanisms. However, our samples sustain nA photocurrents for hours, meaning that these currents cannot be produced by electrochemical reactions or stored charge.

The quantum efficiency of the photoconductivity of porphyrin nanorods can be estimated from the dimensions of the nanorods, the current flowing through them, and the photon flux from the light source. For a 488 nm beam focused to 0.3 mm with a power of 0.78 mW, as used in Figure 2, the photon flux is 2.7×10^{22} photons $\text{m}^{-2} \text{ s}^{-1}$. The total area of the nanorods on the surface was 2.1×10^7 nm^2 based on the assumptions described previously. The maximum current passing through the nanorods was 2.1 nA or 1.3×10^{10} electrons s^{-1} . Therefore, the number of electrons transported per photon striking a nanorod was 0.023 or an electron transport efficiency of 2.3%.

In the formulation of a qualitative conductivity model, three experimental observations must be addressed: (1) the current turns on and off quickly when the light is turned on and off; (2) the photoconductivity (as measured by the current level while the light is on) grows slowly with light exposure and decays slowly when the light is off; and (3) the polarity of the short-circuit photocurrent is trainable by the polarity of the previously applied bias voltage.

In our model, the electron energy levels are spatially localized, perhaps on single molecules or small groups of molecules. For ease of discussion we call these electronic energy levels orbitals and refer to them as we would the orbitals of a single molecule: namely, the HOMO and the LUMO. The high-energy orbitals (the LUMOs) are expected to have greater spatial extent and coupling than the lower energy level orbitals (the HOMOs). In the model, the HOMOs are below the Fermi energy, E_F , of the metal electrodes, and the LUMOs are above E_F . When light is applied, electrons can be photoexcited from the HOMOs to the LUMOs. Because the LUMOs are closely coupled, the electrons can move rapidly and drain out to the lower energy levels in the contact pads. Transport through the LUMOs competes with relaxation from the LUMO back to the HOMO. The main phototransport process is shown in Figure 6. An electron from the left pad moves into an available HOMO at the left end of the nanorod, is photoexcited to the

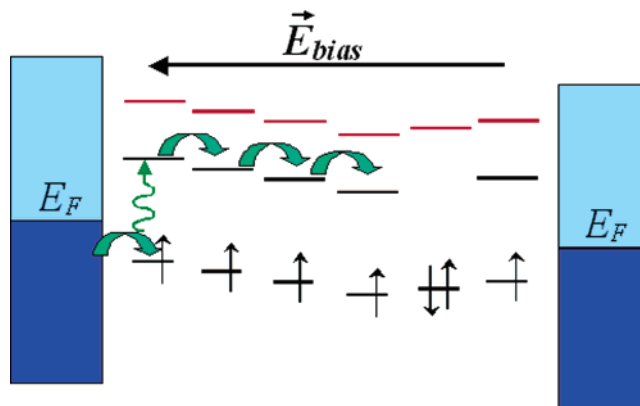


Figure 6. Relative energy levels in qualitative model for photoconductivity with a bias voltage applied. Prior to the instant shown here, one electron from all but one of the HOMOs has been photoexcited to the LUMO, and then has drained away into the electrodes, leaving half-occupied HOMOs. The positive charge left behind creates a curved distribution of energies as shown. Subsequently, electrons entering the HOMO from the left can be photoexcited into the LUMO (as shown) and travel quickly through the tightly coupled LUMOs. Such an electron is unable to move onto a molecular group with a filled HOMO, since the level for the negative ion that would be thus created (shown in red) is higher in energy.

LUMO, and then moves rapidly across the sample through the more closely coupled LUMOs until it is de-excited, is blocked by a molecule with a filled HOMO, or reaches the opposite electrode. This explains the rapid turning on/off of current when the light is turned on/off, since each electron transported must be photoexcited into the LUMO.

When the light is turned off, much slower transfer occurs via hopping through the weakly coupled HOMOs. Filled HOMOs represent an impediment to electron transport since movement of electrons onto molecules with filled HOMOs requires access to the higher-energy negative ion levels shown in red in Figure 6. The filling of the HOMOs when the light is off explains the slow decay of photoconductivity of the nanorods in the dark. By contrast, when light is first applied, a distribution of half-filled HOMOs is rapidly created, allowing conduction as shown by the initial rapid rise of current in Figure 2. In this model, the subsequent gradual increase in photoconductivity is due to a complex interplay between the removal of conduction impediments as more electrons are photoexcited out of filled HOMOs and the recreation of these impediments by refilling of HOMOs from deexcitation of electrons traveling through the LUMOs.

In this model, the zero-bias photocurrent is explained by the development of a built-in field. When a bias voltage is applied, the associated electric field (shown pointing to the left in Figure 6) drives the HOMO electrons toward the right through the weakly coupled chain of HOMOs, leaving net positive charge on the left. When the bias is removed, this asymmetric charge distribution in the HOMOs creates a built-in field pointing in the opposite direction as the previously applied field. In our model, the zero bias photocurrent propagates through the LUMOs, but the electrons are driven by the built-in field instead of the field due to the bias.

In conclusion, we have observed three distinct photoelectronic behaviors in samples of self-assembled porphyrin nanorods: (1) the nanorods only carry current when light is applied, (2) when the light is first applied, the photoconductivity rises quickly, and then grows further on time scales of hundreds of seconds, and (3) under zero applied bias voltage, we observe a sustained photocurrent with a directionality opposite to that of the previously applied bias voltage. We propose a qualitative model which explains the conduction in terms of excitation of electrons from HOMOs to LUMOs, with the LUMOs of previously photoionized molecules providing a conduction path for electrons between the electrodes. Our interpretation of the conductivity results in light of this model has certain consequences that can be tested experimentally. Namely, the application of light to the nanorods should cause them to develop a net positive charge if they are in contact with AuPd electrodes. The slow growth and decay of the photoconductivity are the predicted consequences of this ionization. Under these conditions, this net charge should be observable via electrostatic force microscopy.³³ Furthermore, it should be possible to asymmetrically distribute this charge by application of an external bias, and this effect should also be observable with electrostatic force microscopy.

Acknowledgment. We thank the David and Lucille Packard Foundation, the Camille and Henry Dreyfus Foundation, and the National Science Foundation [CHE-9900403, DBI-0070361, PHY-0103552, and IGERT program DGE-0221664] for funding.

References

- (1) Kosal, M. E.; Suslick, K. S. *J. Solid State Chem.* **2000**, *152*, 87–98.
- (2) Li, L.-L.; Yang, C.-J.; Chen, W.-H.; Lin, K.-J. *Angew. Chem., Int. Ed.* **2003**, *42*, 1505–1508.
- (3) Lin, K.-J. *Angew. Chem., Int. Ed.* **1999**, *38*, 2730–2732.
- (4) Diskin-Posner, Y.; Dahal, S.; Goldberg, I. *Angew. Chem., Int. Ed.* **2000**, *39*, 1288–1292.
- (5) Li, G.; Fudickar, W.; Skupin, M.; Klyszcz, A.; Draeger, C.; Lauer, M.; Fuhrhop, J.-H. *Angew. Chem., Int. Ed.* **2002**, *41*, 1828–1852.
- (6) Wang, H.; Wang, C.; Zeng, Q.; Xu, S.; Yin, S.; Xu, B.; Bai, C. *Surf. Int. Anal.* **2001**, *32*, 266–270.
- (7) Hofkens, J.; Latterini, L.; Vanoppen, P.; Faes, H.; Jeuris, K.; De Feyter, S.; Kerimo, J.; Barbara, P. F.; De Schryver, F. C.; Rowan, A. E.; Nolte, R. J. M. *J. Phys. Chem. B* **1997**, *101*, 10588–10598.
- (8) Drain, C. M.; Batteas, J. D.; Flynn, G. W.; Milic, T.; Chi, N.; Yabloon, D. G.; Sommers, H. *Proc. Natl. Acad. Sci. U.S.A.* **2002**, *99*, 6498–6502.
- (9) Shi, X.; Barkigia, K. M.; Fajer, J.; Drain, C. M. *J. Org. Chem.* **2001**, *66*, 6513–6522.
- (10) Drain, C. M.; Nifiatis, F.; Vasenko, A.; Batteas, J. D. *Angew. Chem., Int. Ed. Engl.* **1998**, *37*, 2344–2347.
- (11) Drain, C. M. *Proc. Natl. Acad. Sci. U.S.A.* **2002**, *99*, 5178–5182.
- (12) Schwab, A. D.; Smith, D. E.; Rich, C. S.; Young, E. R.; Smith, W. F.; de Paula, J. C. *J. Phys. Chem. B* **2003**, *107*, 11339–11345.
- (13) van der Boom, T.; Hayes, R. T.; Zhao, Y.; Bushard, P. J.; Weiss, E. A.; Wasielewski, M. R. *J. Am. Chem. Soc.* **2002**, *124*, 9582–9590.
- (14) Tsuda, A.; Sakamoto, S.; Yamaguchi, K.; Aida, T. *J. Am. Chem. Soc.* **2003**, *125*, 15722–15723.
- (15) Balaban, T. S.; Goddard, R.; Linke-Schaetzel, M.; Leng, J.-M. *J. Am. Chem. Soc.* **2003**, *125*, 4233–4239.
- (16) Haycock, R. A.; Yartsev, A.; Michelsen, U.; Sundström, V.; Hunter, C. A. *Angew. Chem. Int. Ed.* **2000**, *39*, 3616–3619.
- (17) Takahashi, R.; Kobuke, Y. *J. Am. Chem. Soc.* **2003**, *125*, 2372–2373.
- (18) Kuroda, Y.; Sugou, K.; Sasaki, K. *J. Am. Chem. Soc.* **2000**, *122*, 7833–7834.
- (19) Claessens, C. G.; Stoddart, J. F. *J. Phys. Org. Chem.* **1997**, *10*, 254–272.
- (20) Pullerits, T.; Sundström, V. *Acc. Chem. Res.* **1996**, *29*, 381–389.
- (21) Martinez-Planells, A.; Arellano, J. B.; Borrego, C. M.; Lopez-Iglesias, C.; Gich, F.; Garcia-Gil, J. *Photosynth. Res.* **2002**, *71*, 83–90.
- (22) Olson, J. M. *Photochem. Photobiol.* **1998**, *67*, 61–75.
- (23) Vartanyan, A. T. *Sov. Phys. - Semi.* **1968**, *1*, 1261–1265.
- (24) Weigl, J. W. *J. Mol. Spectrosc.* **1957**, *1*, 216–222.
- (25) Gregg, B. A.; Fox, M. A.; Bard, A. J. *J. Phys. Chem.* **1990**, *94*, 1586–1598.
- (26) Kampas, F. J.; Gouterman, M. *J. Phys. Chem.* **1977**, *81*, 690–695.
- (27) Stanbery, B. J.; Gouterman, M.; Burgess, R. M. *J. Phys. Chem.* **1985**, *89*, 4950–4956.
- (28) Liu, C.-y.; Tang, H.; Bard, A. J. *J. Phys. Chem.* **1996**, *100*, 3587–3591.
- (29) Liu, C.-y.; Pan, H.-I.; Fox, M. A.; Bard, A. J. *Chem. Mater.* **1997**, *9*, 1422–1429.
- (30) Liu, C.-y.; Pan, H.-I.; Fox, M. A.; Bard, A. J. *Science* **1993**, *261*, 897–899.
- (31) Fleischer, E. B.; Miller, C. K.; Webb, L. E. *J. Am. Chem. Soc.* **1964**, *86*, 2342–2347.
- (32) Senge, M. O.; Medforth, C. J.; Forsyth, T. P.; Lee, D. A.; Olmstead, M. M.; Jentzen, W.; Pandey, R. K.; Shelnutt, J. A.; Smith, K. M. *Inorg. Chem.* **1997**, *36*, 1149–1163.
- (33) Kano, K.; Fukuda, F.; Wakami, H.; Nishiyabu, R.; Pasternack, R. F. *J. Am. Chem. Soc.* **2000**, *122*, 7494–7502.
- (34) Martin, Y.; Abraham, D. W.; Wickramasinghe, H. K. *Appl. Phys. Lett.* **1988**, *52*, 1103–1105.

NL049421V